Modeling the Static and Dynamic Behavior of Quarter-Wave-Shifted DFB Lasers

Arthur J. Lowery, Adrian Keating, and Casper N. Murtonen

Abstract—**High-coupling ($\kappa L = 3.0$) phase-shifted DFB lasers are studied using a transmission-line laser model (TLLM), which includes spatial hole burning (SHB), the material gain spectrum, refractive index dependence on carrier concentration, and random spontaneous emission. Good agreement for CW spectra is shown with other models and experimental results. Dynamic simulations of laser transients show SHB-induced deterministic mode hopping and chirping at moderate output powers. The effects of mode hopping and chirping on system performance are studied using a laser model combined with a fiber model.**

I. Introduction

HIGH CAPACITY long-haul fiber communications systems require single-mode lasers that remain single-moded even under large-signal modulation, otherwise pulse spreading in dispersive fibers leads to a dispersion penalty [1]. The quarter-wave ($\lambda/4$) shifted distributed-feedback (DFB) laser (Fig. 1) has been designed for single-mode operation [2], [3] and recent results show that high-Bragg-coupling devices can remain single mode at modulation frequencies >17 GHz and at output powers >20 mW [4]–[7]. However, in contrast, both experimental and theoretical results have also shown multimode behavior of high-coupling devices at output powers of only a few milliwatts [8], [9]. Longitudinal spatial hole burning (SHB), which decreases the threshold gain difference between the main mode and the higher-frequency side mode of the grating, is believed to be the cause of the multimode behavior [8]–[10]. However, the reason why some devices are single mode despite SHB has yet to be identified. Prevention of multimode operation is important because it can cause an error-rate floor in high capacity transmission systems [11].

If single-mode operation is obtained, dynamic wavelength chirping during modulation becomes the limit to long-haul system performance [12]. Chirping is a result of the rapidly changing carrier population and the resulting index changes as the laser is modulated [13], [14]. Chirping can also be induced because of the dynamics of longitudinal SHB during modulation [12]. Recent experimental results have shown that chirping may be reduced, to some extent, by the use of MQW materials [15]. However, chirping can never be totally eliminated in directly modulated semiconductor sources, and so it is essential to be able to assess the effects of chirping on system performance.

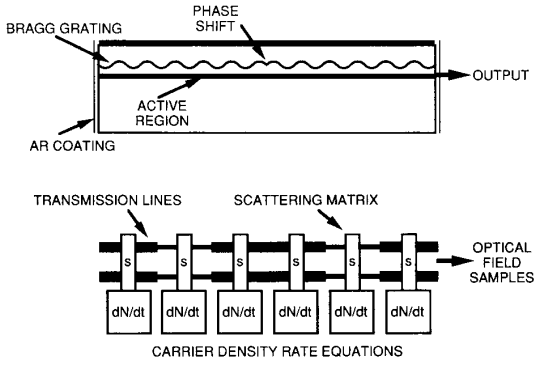

Fig. 1. A quarter-wave-shifted DFB laser and its transmission-line laser model.

A greater understanding of the laser and the mechanisms causing multimode output and chirping can be gained by detailed and accurate laser modeling. This paper presents results for $\lambda/4$-shifted MQW-DFB lasers that show these lasers can remain single mode even under strong modulation because of the spectral selectivity of the MQW material gain. The results were obtained from a comprehensive numerical laser model, the transmission-line laser model (TLLM) [16]. Transmission-line laser models are dynamic, multimode, time-domain models that are able to simulate the dynamic and static spectral and power characteristics of many types of laser, including DFB's [16]–[19].

This paper is divided into six sections. Section II details the DFB laser models including the transmission-line laser model. Section III presents continuous-wave (CW) results for a $\lambda/4$-shifted DFB laser including light–current curves and spectra for a number of output powers and compares these results with previous models and experimental measurements. Section IV details results for a modulated laser and shows SHB induced mode hopping and chirping. Section V demonstrates the use of the laser model with a dispersive-fiber model and shows the effect

Manuscript received August 1, 1991; revised December 2, 1991. This work was supported by OTC, Telecom Australia, the Australian Research Council, and the Australian Telecommunications and Engineering Research Board.

The authors are with the Photonics Research Laboratory, Department of Electrical and Electronic Engineering, University of Melbourne, Parkville, V1C3052, Australia.

IEEE Log Number 9201384.

TABLE I:
ABOVE-THRESHOLD DFB LASER MODELS

Reference	Random Spont. Noise	Multimode	SHB	Threshold Mode Gains	Spectral Plot	Dynamic (small signal)	Dynamic (large signal)	Large Signal Chirp	Gain Spectrum
Soda [8]		yes	yes	yes					
Whiteaway [9]		yes	yes	yes	yes				
Kinoshita [26]			yes	yes		yes	yes	yes	
Agrawal [27]						yes	yes	yes	yes
Vankwikelberge [28], [29]	yes	yes	yes	yes		yes			
Tromberg [30]-[32]	yes		yes	yes		yes			
Libbrecht [33]	yes	yes	yes			yes			
TLLM [16]-[19]	yes	yes	yes		yes	yes	yes	yes	yes

of spectral broadening caused by mode hopping and chirping on pulse spreading. Section VI is the conclusion.

II. DFB LASER MODELS

Table I summarizes the capabilities of above-threshold DFB laser models and includes the characteristics of the TLLM for comparison. Soda *et al.* [8] have solved the coupled-wave equations, which decribe the coupled fields within DFB lasers [20], using F matrices to show that longitudinal SHB can cause the threshold gain difference between the Bragg reflector modes to be reduced to zero at moderate output powers. Reduction of the threshold gain difference produces a multimode spectrum, though spectra were not generated in Soda's model. Realistic multimode spectra have been generated by Whiteaway *et al.* [9]. Their transfer-matrix approach, based on the below-threshold work of Bjork and Nilsson [21], linearizes the parameters in small sections of the DFB and solves the coupled-mode equations in each section. Effects of multiple electrodes [22], the introduction of several phase discontinuities [23], longitudinal variation of the coupling coefficient [24], and stripe width [25] have also been examined using transfer matrices.

Dynamic models, used to predict frequency chirping, usually require time-stepping of the solution, which can be computer-intensive if the spectrum is also solved at each time step by stepping in the wavelength domain. Kinoshita and Matsumoto [26] perform a dynamic analysis using modified rate equations. The longitudinal carrier density is represented by a Fourier series of spatial harmonics. Their model is single mode and thus cannot accurately determine SHB due to multiple modes. However, they conclude that SHB significantly affects chirping and time-resolved chirp waveforms are given for a number of structures.

Other dynamic DFB models include the work of Agrawal [27], who has modeled single-mode nonlinear dynamics, using modified Fabry-Perot laser rate equations. However, although large-signal chirping was modelled, SHB was not considered. Vankwikelberg *et al.* have developed a general-purpose dynamic matrix-based model that includes SHB. They analyze operation at a particular bias point and then perform small-signal ac analysis and noise analysis. Novel devices structures for reduced SHB have been studied [24], but large signal modulation was not evaluated. Tromberg *et al.* [30]-[32] apply classical transmission-line theory to the laser cavity, allowing algebraic evaluation of spatial inhomogeneities [32] and modulation dynamics [33]. However, only single-mode small-signal results have been generated. A large-signal *time-domain* model that includes SHB has been announced by Libbrecht *et al.* [33]. Only FM-modulation response results have been presented as yet.

Fiber communication system models, where the time-domain output of a digitally modulated laser model is fed into a fiber model have been presented by many authors [34], [35]. However, most system models use a single-mode representation of the laser, based on a solution of the rate equations for Fabry-Perot lasers [35]. These equations do not include multimode effects, nor do they include SHB or its effects on chirping and the transient response.

A DFB model that is capable of predicting multimode, dynamic spectra, that includes laser chirp and a material gain spectrum, is the transmission-line laser model (TLLM) [16]. Examination of Table I shows that the TLLM contains all the features of previous DFB laser models except that the threshold gains for each mode are not explicitly calculated. Also, the TLLM is readily incorporated into system models.

Transmission-line laser modeling was originally developed to study the dynamic characteristics of Fabry-Perot lasers [36]. However, recent work has extended the method to cover DFB lasers [17]-[19]. TLLM uses a one-dimensional (1-D) transmission-line analog to the laser cavity as shown in Fig. 1. Voltage pulses, representing the optical traveling waves, travel along the transmission lines and are scattered at scattering nodes S. The scattering represents the stimulated emission and its wavelength dependence, attenuation, and spontaneous emission.

All transmission lines are one-timestep long to ensure that wave samples entering the line sections will simultaneously exit the line sections. Impedance discontinuities between the sections represent the index modulation of the grating of the DFB laser. The transmission-line sections can be a multiple of the length of a grating period [18]. This allows a large time step to be used (a fraction

of a picosecond), giving reasonable computational efficiency: none of the simulations in this paper took more than 10 min on a Sun Sparcstation-2.

The carrier dynamics within the active region are represented by rate-equation models of the local carrier concentration within each section. The simulated emission rate is calculated from the average photon density within a section, which is related to the incident traveling waves to that section and the local carrier concentration. Gain nonlinearity is included in the model to obtain an accurate transient response to current steps [37]. The local effective refractive index is also calculated from the local carrier density [18]. The use of a carrier rate equation for each model section allows carrier-induced inhomogeneities in gain and index to be included. Carrier induced index inhomogeneities are especially important in DFB lasers because they affect the local Bragg wavelength (the peak wavelength) of the grating.

Spontaneous emission noise is introduced into the model as random current sources with Gaussian distributions, one for each wave direction at every section. The standard deviation of these sources is related to the radiative recombination rate to give the correct spontaneous emission power both below and above threshold [19], [38]. The use of a random noise source allows relative intensity noise, turn-on jitter, and mode hopping to be studied without modification of the model [39].

III. CW Characteristics

Although the TLLM is primarily a dynamic model suited to the study of transient phenomena, CW characteristics can be obtained by allowing the turn-on transient to settle before logging results. In this section, the power–current characteristics and the CW spectral characteristics of a high-coupling ($\kappa L = 3.0$) laser with antireflection coated facets are compared with results from other models and experimental results. $\kappa L = 3.0$ lasers have lower threshold currents and linewidths than lasers with a lower κL [7]. However, Whiteaway *et al.* [9] and Soda *et al.* [8] have shown that there is a larger SHB in high-coupling lasers because of a larger longitudinal variation in photon density. Table II shows the laser parameters used in all the simulations. These were taken from Whiteaway *et al.* [9] to allow comparison between his models and the TLLM. Note that the phase shift is in the centre of the device. In all cases, a 42-section TLLM with a timestep of 0.1175 ps was used. Gain nonlinearities were included into the TLLM model to provide the correct damping of transients [37], [39]. The gain compression term was found not to affect the CW results from the model.

A. Output Power Versus Bias Current

The simulations were performed with sufficient iterations for the turn-on transient to settle. The output power was obtained by squaring and averaging the optical field samples from one facet of the model. The averaging was over 10 000 timesteps to reduce the intensity noise for each injection current level. The output power versus injection current is shown in Fig. 2(a) and the differential efficiency in Fig. 2(b). Also plotted are results from a single-mode solution of the coupled-wave equations including SHB that we developed, which is similar to [28].

The light–power versus current curves [Fig. 2(a)] indicate a reasonable agreement between the TLLM and the coupled-wave model. However, the coupled-wave model slightly underestimates the output power at higher injection currents. This is because a second mode grows at

TABLE II:
DFB Laser Parameters

Symbol	Parameter Name	Value	Unit
λ	Wavelength	1.55	μm
L	Laser cavity length	400.0	μm
w	Active stripe width	3.5	μm
d	Active region depth	0.18	μm
$a\Gamma$	Gain cross section × waveguide confinement factor	1.05×10^{-16}	cm^2
N_0	Transparency carrier density	1.5×10^{18}	cm^{-3}
ϵ	Gain compression factor	6×10^{-17}	cm^3
$\bar{n}_e$	Group index of waveguide	3.7	
α	Henry's linewidth factor	4.86	
τ_s	Carrier lifetime	4.0	ns
α_{sc}	Waveguide attenuation	40.0	cm^{-1}
β	Spontaneous coupling per longitudinal mode	1.24×10^{-5}	
κL	Grating coupling constant	3.0	

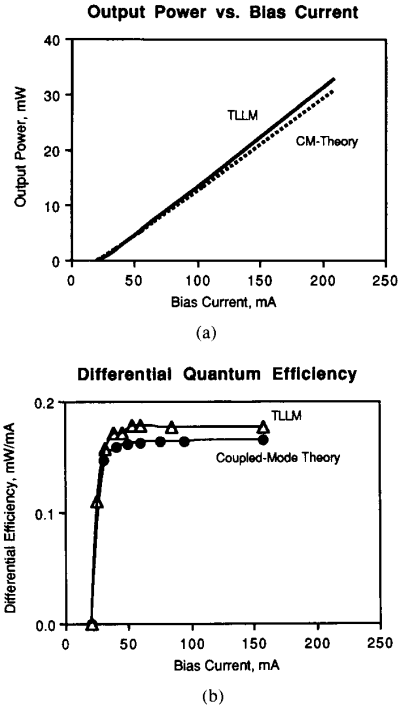

Fig. 2. (a) Output power versus bias current calculated with the TLLM and with a single-mode solution of the coupled-wave equations including SHB. (b) Differential efficiency versus bias current calculated with the TLLM and with a single-mode solution of the coupled-wave equations including SHB.

higher currents and this mode has a different efficiency to the main mode. The threshold current is approximately 21 mA, which is in reasonable agreement with experimental results for high coupling DFB lasers [15]. Whiteaway gives the optical power for bulk lasers at 28 mA as 0.37 mW per facet, much below the 0.8 mW obtained with our models. The differential efficiency curves again show a reasonable agreement between the TLLM and the coupled-wave model. Both models show a small superlinearity at currents up to 63 mA (3× threshold). Note that the linearity is dependent on κL and that sublinearity could be obtained with $\kappa L \leq 1.25$. The efficiency of approximately 0.17 mW/mA is in good agreement with experimental measurements of between 0.15 and 0.20 mW/mA for high coupling MQW lasers [15, 7]. Note that the gain cross section a multiplied by the confinement factor Γ is similar for bulk and MQW lasers, so that our efficiency comparison is valid.

B. CW Spectra versus Bias Current

Whiteaway has produced CW spectral plots for $\kappa L = 3.0$ laser that show a transition to multimode spectra at moderate output powers [9]. The transmission-line laser model was run with his parameters to enable a direct comparison to be made. In all cases the spectra were obtained using 32K point Fourier transform of the optical field samples after the transient had settled. The Fourier transform output was smoothed using a Gaussian function with $\sigma = 4.2$ GHz to remove noise caused by the random spontaneous emission and to obtain a similar wavelength resolution to Whiteaway.

Fig. 3 shows the spectra at drive currents of 28 and 63 mA. The 28 mA spectrum [Fig. 3(a)] has the same features as Whiteaway's simulation [9] with a dominant TE0 mode at the center of the Bragg stopband and a smaller TE+1 side mode. However, the side mode has less power in the TLLM simulation than in Whiteaway's simulations. At 63 mA [Fig. 3(b)] the modes had almost equal powers: Whiteaway predicted equal mode powers. Whiteaway's spectra have a 17 dB higher noise floor, away from the Bragg wavelength. This indicates that more spontaneous emission is generated in his model than in the TLLM, although the parameters defining spontaneous emission are identical in the two models. We checked our amplified spontaneous emission (ASE) power below threshold and found it to agree with ASE theory [19]. Increasing our spontaneous emission factor by 17 dB [Fig. 3(c)] gave excellent agreement with Whiteaway's 28 mA spectrum but increased the intensity noise to unrealistic levels [39].

Whiteaway predicted a zero SMSR at >5 mW output power in bulk lasers, in contrast to recent experimental results that show that a SMSR of >40 dB can be obtained at powers >30 mW with $\kappa L = 3.0$ MQW lasers [5], [7], [15]. We repeated our simulations but included material gain, approximated as a fixed-wavelength Lorentzian filter centred at the central mode of the laser with a half

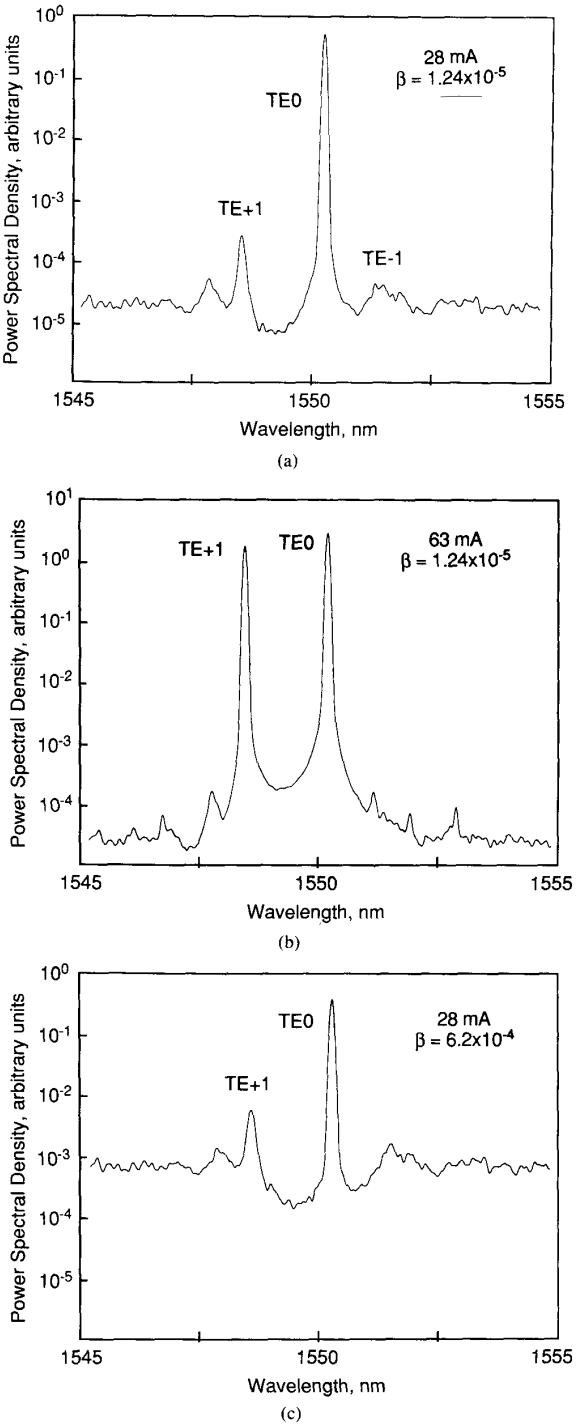

Fig. 3. CW spectra calculated with the TLLM with a flat gain spectrum for: (a) 28 mA bias, (b) 63 mA bias, and (c) 28 mA bias with 17 dB more spontaneous emission.

width of approximately 10 nm. This narrow-gain bandwidth giving good selectivity between the TE0 mode and the shorter-wavelength TE+1 mode is a reasonable ap-

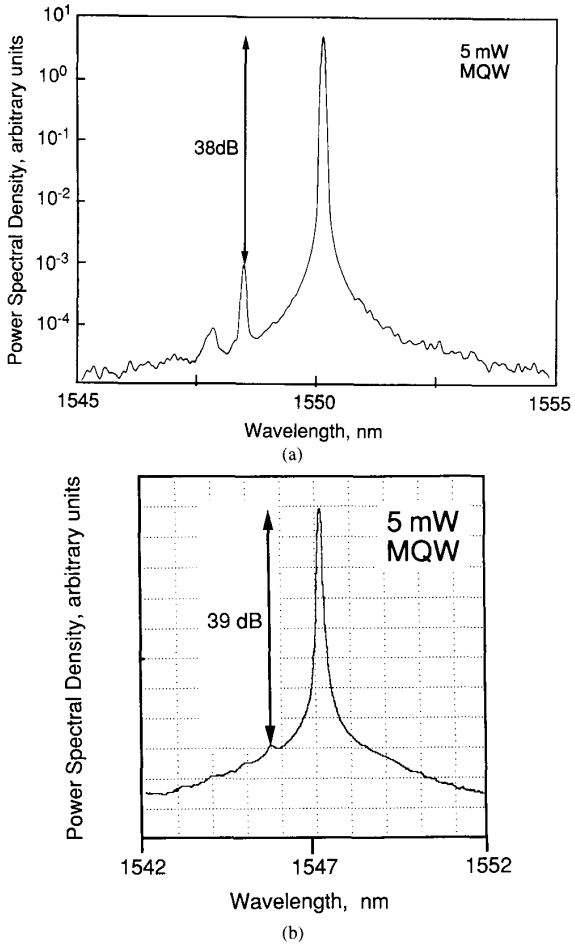

Fig. 4. (a) Calculated CW spectrum assuming a 10 nm FWHM gain spectrum and 63 mA bias (5 mW). (b) Measured CW spectrum of a MQW-DFB laser at 5 mW.

proximation to that obtained with MQW materials [40]. As shown in Fig. 4(a) the material gain kept the laser single-mode (SMSR >38 dB) at three times threshold (63 mA) or about 5 mW. Fig. 4(b) shows the measured spectrum of a Hitachi MQW-DFB laser with similar parameters again at 5 mW. This has a single-mode spectrum with a SMSR of 39 dB. Note that the limited wavelength resolution of the monochromator has made the side mode difficult to observe. We also modeled the laser when the material gain peak was placed longer wavelengths. In this case, the laser remained single mode for displacements up to 4 nm after which a TE−1 mode appeared. Shifts in the gain peak to shorter wavelengths favored the SHB-induced TE+1 mode. These examples show that it is essential to include the material gain spectrum in DFB laser models.

C. Side-Mode Suppression Ratio (SMSR) versus Bias Current

The SMSR's for 1) the TLLM with no material gain spectral dependence, 2) the TLLM with material gain spectral dependence, and 3) from Whiteaway's model are plotted in Fig. 5. These results show that good control of the material gain peak position, with respect to the Bragg wavelength, as was obtained by MQW structures in [26] can improve the SMSR of DFB lasers at high output powers. The simulations with flat material gain showed very poor SMSR at moderate powers, confirming the importance of material gain spectral dependence in mode selection. Note that Uomi *et al.* ascribe the high SMSR of their lasers to the low (approx. 4.0) linewidth enhancement factor of their MQW material [5]. Our results were from a laser with a similar linewidth enhancement factor of 4.86 and therefore indicate that the well-positioned narrow-gain spectrum obtained with MQW material is more likely the cause of a high SMSR in their experiments.

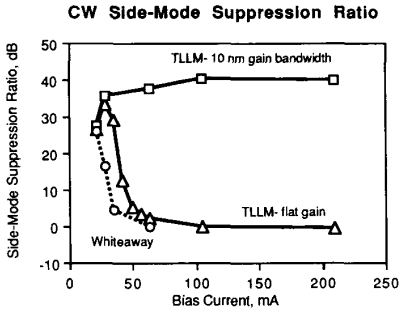

Fig. 5. Side-mode suppression ratio (SMSR) versus bias current: (a) TLLM with flat material gain, (b) TLLM with 10 nm FWHM material gain bandwidth, (c) Whiteaway's results.

D. Longitudinal Carrier Density

The variation of carrier density along the length of the cavity due to SHB, is plotted in Fig. 6. At 21 mA there is minimal spatial hole burning because the laser is at threshold. At 28 mA (2 kA/cm^2) the maximum carrier density is 2.40×10^{18} cm^{-3} and the minimum carrier density, at the center of the device is 1.89×10^{18} cm^{-3}. These densities compare with 2.39×10^{18} cm^{-3} and 1.94×10^{18} cm^{-3} in Whiteaway's model [9]. The discrepancies could be due to the use of 42 model sections in the TLLM against eight sections in Whiteaway's model. At 63 mA (4.5 kA/cm^2) the maximum carrier density in the TLLM was 2.6×10^{18} cm^{-3} and the minimum was 1.92×10^{18} cm^{-3}, compared with 3.15×10^{18} cm^{-3} and 1.95×10^{18} cm^{-3} in Whiteaway's model. Our single-mode solution of the coupled-mode equations gave similar carrier densities to the TLLM.

IV. Dynamic Spectra

All spectral broadening mechanisms, including laser chirp and multiple modes, can adversely affect the performance of fiber communications systems because of pulse spreading in the fibers [12], [26]. This section shows that hopping between multiple modes and laser chirp are significantly affected by SHB. All simulations in this section used a flat material gain to demonstrate mode hop-

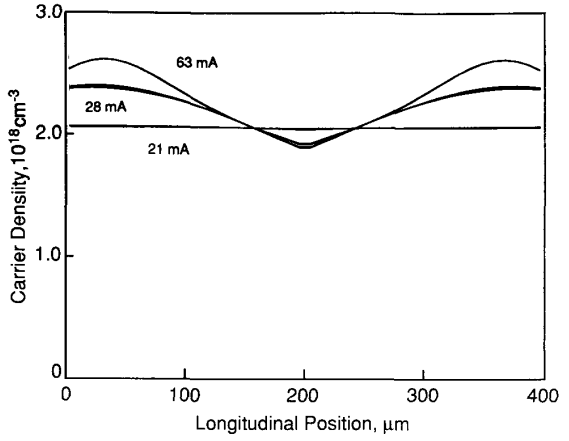

Fig. 6. Carrier density versus longitudinal position at three bias currents. The line thickness indicates noise-induced temporal variations in the carrier density.

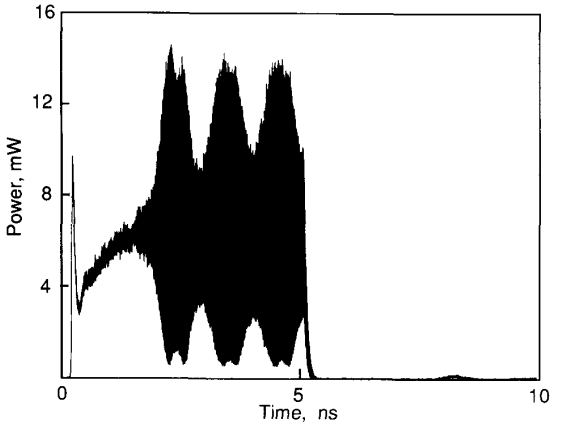

Fig. 7. Simulated laser power for a 5 ns pulse of 63 mA followed by a 5 ns pulse of 21 mA from a bias level of 21 mA.

ping between during transients. Random spontaneous emission noise sources were included in all simulations.

A. Multimode Characteristics

Fig. 7 shows the dynamic response of the laser to a 5 ns pulse of 63 mA followed by a 5 ns pulse of 21 mA. The laser was initially biased at 21 mA. The resulting optical pulse shows an initial transient followed by a slower growth in power, then a large oscillation in power. The initial transient is common to all lasers. The slow rise in power after this transient is caused by the onset of spatial hole burning, which gave the super-linear characteristic in Fig. 2. The large oscillation is a result of beating between the two laser modes, and is is at approximately 200 GHz. The strength of this beating varies cyclically, suggesting a cyclic variation in the relative powers of the modes.

Fig. 8 shows a plot of the carrier concentrations during the pulses of Fig. 7 at (a) 48 μm from the end of the cavity

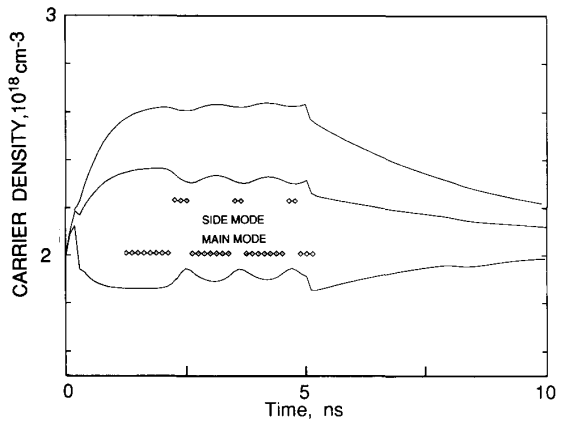

Fig. 8. Variation of the carrier density at three points along the cavity during the pulse in Fig. 7. (a) 42 μm, (b) 114 μm, (c) center. The points indicate the dominant mode during the pulse.

(position of maximum carrier density); (b) 114 μm from the end of the cavity, (c) the middle of the cavity. The middle of the cavity suffers most spectral hole burning, which recovers during the 21 mA bias period. All three plots have cyclic fluctuations during the time of the mode beating. The phase of the fluctuations of curve (b) are opposite to the those of (c). These fluctuations can be explained by the intensity profiles of the main and side-mode extracting carriers at different points along the laser. The main mode has maximum intensity at the center of the device: the side mode has maximum intensity about 114 μm from the facets.

Spectral analysis revealed that the main mode grew first, saturating the center of the cavity. This saturation caused the gain of the main mode to decrease, and the side mode to increase, in power. The side-mode then extracted carriers in its intensity peaks, reducing its gain. The main mode then regained dominance. This mode hopping continued until the drive current was reduced below threshold. A plot of the mean wavelength of the modeled lasing spectrum against time is shown as dots in Fig. 8 and clearly indicates mode hopping. Continuation of the 63 mA bias showed that the cyclic mode hopping settled down after approximately 20 ns. At this time, the mode powers were almost equal.

In practice, mode hopping can be minimized by ensuring a high CW SMSR. However, there is always a statistical probability that the side-mode will grow to dominance, because of the randomness of the spontaneous emission noise. It is therefore essential to have a model that can simulate mode hopping.

B. Time-Resolved Chirping

Kinoshita and Matsumoto have shown theoretically that SHB significantly affects the time-resolved dynamic spectra of DFB lasers, leading to a slow chirp towards shorter wavelengths for $kL = 1.0$ lasers during the period after the transient the laser [26]. This chirp is due to the redis-

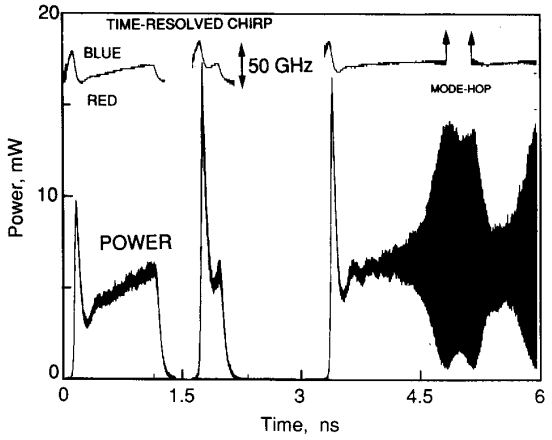

Fig. 9. Simulated laser power (a) and time-resolved frequency (b), for a bit-sequence of 111010001111111 at 2.5 Gbps.

tribution of the longitudinal carrier density after the initial transient peak. They also a predicted a shift towards longer wavelengths for high-kL lasers. Bergano has measured a drift to *longer* wavelengths during successive '1' pulses [41]. However, this drift was explained by junction heating and not SHB.

We simulated a laser driven by a bit-sequence of 111010001111111 at 2.5 Gbps with 63 mA for 1-pulses and 21 mA for 0-pulses. The power and the time-resolved chirp waveforms are shown in Fig. 9. The laser chips blue to red by approximately 35 GHz during the initial transient of each pulse. A red-blue chirp of 20 GHz over about 1 ns then occurs only during the first pulse. This red-blue chirp is a result of the hole burning that occurs during the first pulse and is consistent with the red to blue CW wavelength shift as the laser current is slowly increased [9]. The later pulses do not experience this red-blue chirp because the carrier profile has not had time to recover; the recovery time is approximately 5 ns [Fig. 8(b)]. The recovery time is probably governed by the carrier lifetime which was 4 ns. Note that the laser mode hops during the long sequence of ones.

V. Pulse Spreading in Dispersive Fiber

One aim of simulating the static and dynamic spectra of DFB lasers is to be able to estimate their performance in fibre communication systems. Henmi *et al.* have studied the effect of submode oscillation on system performance, in particular on the error-rate-floor [11] and have concluded from their observations that a large threshold gain difference is required between the modes to reduce the probability of the submode oscillation causing errors. They have specified an adequate gain difference between the modes for adequate system performance using a simple Fabry–Perot formula. Yamamoto *et al.* have made simple estimates of system performance using linear approximations to the measured chirp waveform and Gaussian approximations to the pulse shape from DFB lasers [12]. More complete system models, including laser and fiber models, usually approximate the chirping of a single-mode laser (i.e., a DFB) to that of a Fabry–Perot laser to allow a single-mode rate-equation description [35].

The TLLM can form the basis of a system model with few assumptions, in contrast to earlier DFB system models, by adding a dispersive fiber model to the output of the DFB TLLM. A dispersive fiber model involves convolution the output field samples from the laser model with the impulse response of the fiber [35]. The resulting model can cope with the multimodel, chirped spectra as produced by the DFB laser model.

In all tests the laser was biased at 21 mA and the initial carrier density was flat. The laser was driven with a repeated 101010 $\cdots$ sequence of bits for 10 ns at a rate of 2.5 Gbps. The total drive current for a 1-pulse was 63 mA.

A. Simulation with 10 nm Material Gain Bandwidth

Fig. 10(a) shows the simulated output of a MQW-DFB laser with a 10 nm FWHM gain spectrum. Each pulse has a sharp transient peak followed by a dip and a slower recovery, as explained in Fig. 7. The shape and power of the pulses evolves during the first three pulses as spatial hole burning occurs with a time constant of about 1 ns. Note that the recovery time constant for SHB is much longer than the pulse-to-pulse spacing so that no appreciable recovery occurs between pulses.

Fig. 10(b) shows the pulse after they have propagated through 7 km fiber with a dispersion of 18 ps/nm $\cdot$ km (blue faster than red). Because of the large blue-to-red chip of the transient peak of each pulse, this peak is spread in time, with a corresponding decrease in peak power. The recovery after the dip, however, has a red-to-blue chirp due to the SHB [26] and so is compressed in time. The inset time averaged chirp spectrum shows a good suppression of the side mode and a -10 dB chirp width of approximately 50 GHz.

Fig. 10(c) shows the pulses of Fig. 10(a) after propagating through 35 km of the same fiber. The initial peaks of the pulses have now spread into the previous 0-data bits and the trailing-edges of the pulse have spread forward into the following 0-data bits. Note that the chirp of the pulses' peaks is greater than the SHB-induced chirp, and dominates in this simulation because the SHB-chirp only occurs during the first few pulses. However, in pulse sequence with long (>1 ns) series of ones followed by longer (>5 ns) series of zeros, SHB-induced chirp is likely to produce further dispersion. This behavior would cause a large power penalty in bandwidth-limited receivers and is much more complex than the approximations used in [12].

B. Simulation with Flat Material Gain

Fig. 11(a) shows the simulated ouptut of a laser with a flat gain spectrum with the same drive conditions as in Fig. 10(a). Some of the pulses have a very fast ringing

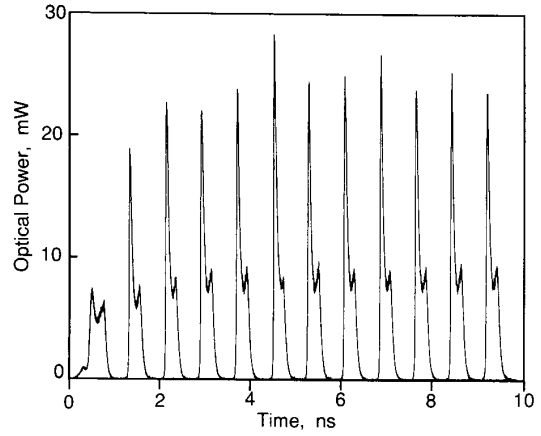

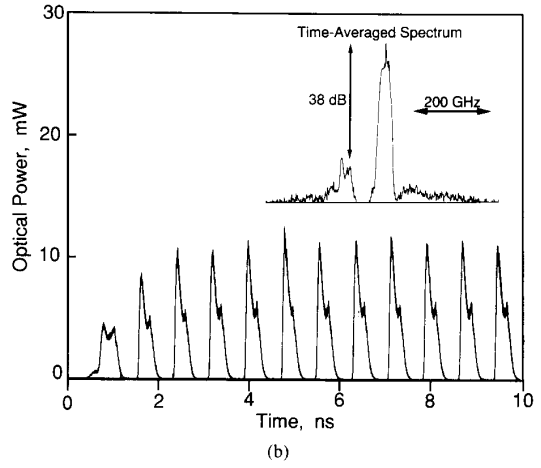

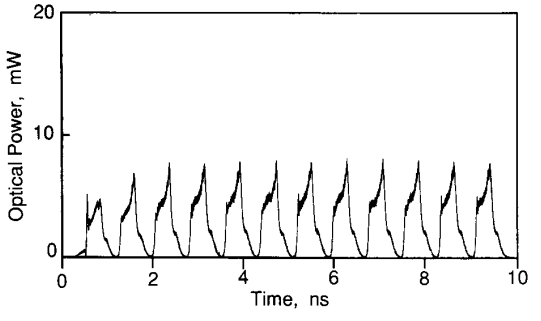

Fig. 10. (a) Simulated laser power for a 101010 · · · bit sequence at 2.5 Gbps with a material gain bandwidth of 10 nm, 63 mA pulse current, and 21 mA bias current. (b) Output pulses after pulses in (a) have propagated through 7 km of fiber (18 ps · nm^{-1} · km^{-1}). The time averaged spectrum is shown in the inset. (c) As (b) but with 35 km fiber.

during their peaks. Fourier analysis revealed that this ringing is due to a beating between the main mode and the side mode. Note that this multimode behavior only occurs after SHB has taken place; the first few pulses are single mode. The inset in Fig. 11(b) clearly shows the presence of the side mode with an SMSR of 20 dB. This

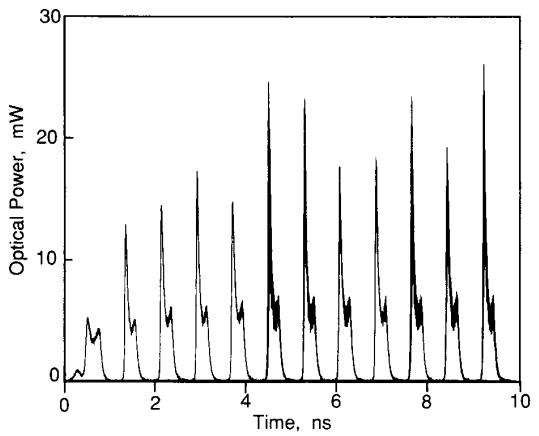

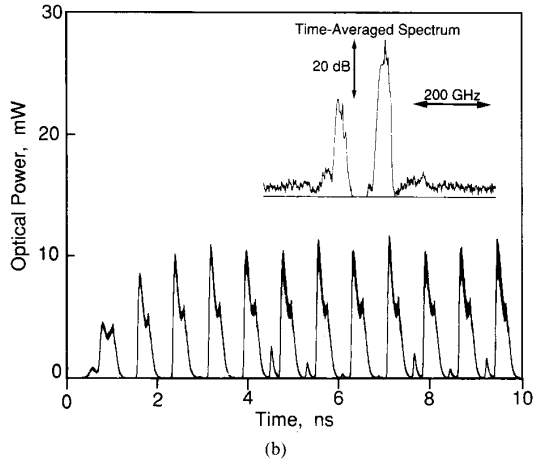

Fig. 11. (a) Simulated laser power for a 101010 · · · bit sequence at 2.5 Gpbs with a flat material gain, 63 mA pulse current, and 21 mA bias current. (b) Output pulses after pulses in (a) have propagated through 7 km of fiber (18 ps · nm^{-1} · km^{-1}). The time averaged spectrum is shown in the inset.

dynamic SMSR is better than the CW SMSR shown in Fig. 3(c).

Fig. 11(b) shows the pulses after they have propagated through 7 km of fiber. The main pulses have similar features to be propagated single-mode pulses in Fig. 10(b), however, small pulses are present during 0-bits. These small pulses correspond the initial peaks of the main pulses where Fourier analysis revealed there was a power in the side mode: this side-mode power has been shifted forward in time into the previous 0-bit time slot. Similar effects have been observed by Henmi *et al.* [11].

An approximate calculation from the dispersion parameter, the difference in wavelength between the two modes, and the fiber length, shows that the forward shift is approximately 200 ps. This shift is enough to place the initial peak of a 1-pulse at the centre of a 0-bit slot. Such an occurrence could produce a receiver error-rate floor, although the probability of such an error could be reduced by matching the material gain spectrum to the Bragg

wavelength [11]. Error rate floors have been observed when multimode DFB lasers were used with only 7 km of nondispersion shifted fiber at 2.4 Gbps [1]. This example illustrates the importance of a multimode model when simulating system performance; a single-mode laser model would not predict such error-rate floors.

VI. Conclusion

We have shown that the transmission-line laser model is able to simulate the static and dynamic spectral and power characteristics of quarter-wave-shifted DFB lasers. Specifically, we have shown that for our laser parameters:

1) The simulated optical-power versus current characteristics are in good agreement with a single-mode solution of the coupled-wave equations including SHB and experimental results.
2) the model predicts a superlinear optical power versus current curve,
3) the CW spectra show a transition to a multimode spectrum at moderate output powers if the material gain is assumed to be flat,
4) the CW spectra are in reasonable agreement with those obtained using a multimode frequency-domain transfer-matrix model, such as that of Whiteaway *et al.* However, the spontaneous emission rate appears to be excessive in Whiteaway's model,
5) inclusion of the material gain spectrum into the model gives single-mode spectra at high powers that are in agreement with experimental measurements if the gain peak wavelength is at the dominant mode or up to +4 nm above it,
6) SMSR's of better than 37 dB can be obtained at output powers up to 30 mW if the material gain is as above,
7) the time constant for SHB to occur is approximately 1 ns at 5 mW output and the longitudinal carrier profile takes more than 5 ns to recover from SHB, the recovery time being governed by the carrier lifetime,
8) hopping between the main mode and the side mode can occur after transients when a flat gain is assumed and the hopping is initially deterministic,
9) the laser chirps by more than 20 GHz during the onset of SHB,
10) chirping limits the transmission distance to less than 35 km with 18 ps/nm · km dispersion fiber for a single-mode laser at 2.5 Gbps,
11) mode hopping limits the transmission distance to be less than 7 km with 18 ps/nm · km dispersion fiber for a single-mode laser at 2.5 Gbps,
12) the system simulations are in good agreement with measurements.

Thus, we have demonstrated the TLLM to be an accurate and useful design tool for DFB lasers and optical communication systems.

Acknowledgment

We would like to thank J. Whiteaway of Bell Northern research, Harlow, Essex, for providing detailed results from his model and K. Uomi of Hitachi Central Research Laboratory, Japan, for providing the laser. Also, OTC and Telecom Australia's permission to publish this paper is acknowledged.

References

[1] S. Sasaki, M. M. Choy, and N. K. Cheung, "Effects of dynamic spectral behaviour and mode-partitioning of 1550 nm distributed feedback lasers on Gbit/s transmission systems," *Electron. Lett.*, vol. 24, pp. 26-28, 1988.
[2] H. A. Haus and C. V. Shank, "Antisymmetric taper of distributed feedback lasers," *IEEE J. Quantum Electron.*, vol. QE-11, pp. 154-161, 1975.
[3] K. Utaka, S. Akiba, K. Sakai, and Y. Matsushima, "λ/4-shifted InGaAsP/InP DFB lasers," *IEEE J. Quantum Electron.*, vol. QE-22, pp. 1042-1051, 1986.
[4] K. Uomi, H. Nakano, and N. Chinone, "Ultrahigh-speed 1.55 μm λ/4-shifted DFB lasers with a bandwidth of 17 GHz," *Electron. Lett.*, vol. 25, pp. 668-669, 1989.
[5] M. Aoki, K. Uomi, T. Tsuchiya, S. Sasaki, and N. Chinone, "Stabilization of the longitudinal mode against spatial hole burning in λ/4-shifted DFB lasers by quantum size effect," *IEEE Photon. Technol. Lett.*, vol. 2, pp. 617-619, 1990.
[6] K. Uomi, M. Aoki, T. Tsuchiya, M. Suzuki, and N. Chinone, "Dependence of relaxation oscillation frequency and damping *K* factor on the number of quantum wells in 1.55 μm InGaAsP DFB lasers," *IEEE J. Quantum Electron.*, to be published.
[7] K. Uomi, S. Sasaki, T. Tsuchiya, and M. Okai, "Spectral linewidth reduction by low spatial hole burning in 1.5 μm multi-quantum-well λ/4-shifted DFB lasers," *Electron. Lett.*, vol. 26, pp. 52-53, 1990.
[8] H. Soda, Y. Kotaki, H. Sudo, H. Ishikawa, S. Yamakoshi, and H. Imai, "Stability in single longitudinal mode operation in GaInAsP/InP phase-adjusted DFB lasers," *IEEE J. Quantum Electron.*, vol. QE-23, pp. 804-814, 1987.
[9] J. E. Whiteaway, G. H. B. Thompson, A. J. Collar, and C. J. Armistead, "The design and assessment of λ/4 phase-shifted DFB structures," *IEEE J. Quantum Electron.*, vol. 25, pp. 1261-1279, 1989.
[10] M. Usami and A. Shigeyuki, "Suppression of longitudinal spatial hole-burning effect in λ/4-shifted DFB lasers by non-uniform current distribution," *IEEE J. Quantum Electron.*, vol. 25, pp. 1245-1253, 1989.
[11] N. Henmi, Y. Koizumi, M. Yamaguchi, M. Shikada, and I. Mito, "The influence of directly modulated DFB LD sub-mode oscillation on long-span transmission systems," *J. Lightwave Technol.*, vol. 6, pp. 636-642, 1988.
[12] S. Yamamoto, M. Kuwazuru, H. Wakabayashi, and Y. Iwamoto, "Analysis of chirp power penalty in 1.55 μm DFB-LD high-speed optical fiber transmission systems," *J. Lightwave Technol.*, vol. LT-5, pp. 1518-1524, 1987.
[13] A. J. Lowery, "A model for picosecond dynamic laser chirp based on the transmission line laser model," *IEE Proc., J; Optoelectron.*, vol. 135, pp. 126-132, 1988.
[14] L. D. Westbrook, I. D. Henning, A. W. Nelson, and P. J. Fiddyment, "Spectral properties of strongly-coupled 1.5 μm DFB laser diodes," *IEEE J. Quantum Electron.*, vol. QE-21, pp. 512-518, 1985.
[15] K. Uomi, T. Tsuchiya, H. Nakano, M. Aoki, M. Susuki, and N. Chinone, "High-speed and ultra-low chirp 1.55 μm multiquantum well λ/4-shifted DFB lasers," *IEEE J. Quantum Electron.*, vol. 27, pp. 1705-1713, 1991.
[16] A. J. Lowery, "Transmission-line modelling of semiconductor lasers: the transmission-line laser model," *Int. J. Numer. Model.*, vol. 2, pp. 249-265, 1990.
[17] ——, "Dynamic modelling of distributed-feedback semiconductor lasers using scattering matrices," *Electron. Lett.*, vol. 25, pp. 1307-1308, 1989.

[18] ——, "A new dynamic model for multimode chirp in DFB semiconductor lasers," *IEE Proc. J: Optoelectron.*, vol. 137, pp. 293–300, 1990.
[19] ——, "Amplified spontaneous emission in semiconductor laser amplifiers: The validity of the transmission-line laser model," *IEE Proc. J: Optoelectron.*, vol. 137, pp. 241–247, 1990.
[20] H. Koglenik and C. V. Shank, "Coupled-wave theory of distributed feedback lasers," *J. Appl. Phys.*, vol. 43, pp. 2325–2335, 1972.
[21] G. Bjork and O. Nilsson, "A new exact and efficient numerical matrix theory of complicated laser structures: Properties of asymmetric phase-shifted DFB lasers," *J. Lightwave Technol.*, vol. LT-5, pp. 140–146, 1987.
[22] K. Kikuchi and H. Tomofuji, "Analysis of oscillation characteristics of separated-electrode DFB laser diodes," *IEEE J. Quantum Electron.*, vol. 26, pp. 1717–1727, 1990.
[23] S. Ogita, Y. Kotaki, M. Matsuda, Y. Kuwahara, and H. Ishikawa, "Long-cavity multiple-phase-shift distributed feedback laser diode for linewidth narrowing," *IEEE J. Quantum Electron.*, vol. 26, pp. 1596–1603, 1990.
[24] G. Morthier, K. David, P. Vankwikelberge, and R. Baets, "A new DFB-laser diode with reduced spatial hole burning," *IEEE Photon. Technol. Lett.*, vol. 2, pp. 388–390, 1990.
[25] K. Taka, Y. Nakano, and A. Ushirokawa, "Proposal of a distributed feedback laser with nonuniform stripe width for complete single-mode oscillation," *Electron. Lett.*, vol. 20, pp. 82–84, 1984.
[26] J-I. Kinoshita and K. Matsumoto, "Transient chirping in distributed feedback lasers: effect of spatial hole-burning along the laser axis," *IEEE J. Quantum Electron.*, vol. 24, pp. 2160–2169, 1988.
[27] G. P. Agrawal, "Effect of gain and index nonlinearities on single-mode dynamics in semiconductor lasers," *IEEE J. Quantum Electron.*, vol. 26, pp. 1901–1909, 1990.
[28] P. Vankwikelberge, G. Morthier, and R. Baets, "CLADISS—A longitudinal multimode model for the analysis of the static, dynamic, and stochastic behavior of diode lasers with distributed feedback," *IEEE J. Quantum Electron.*, vol. 26, pp. 1728–1741, 1990.
[29] P. Vankwikelberge, F. Buytaert, A. Franchois, R. Baets, P. I. Kuindersma, and C. W. Fredriksz, "Analysis of the carrier-induced FM response of DFB lasers: theoretical and experimental case studies," *IEEE J. Quantum Electron.*, vol. 25, pp. 2239–2254, 1989.
[30] B. Tromborg, H. Olesen, X. Pan, and S. Saito, "Transmission line description of optical feedback and injection locking for Fabry–Perot and DFB lasers," *IEEE J. Quantum Electron.*, vol. QE-23, pp. 1875–1889, 1987.
[31] X. Pan, H. Olesen, and B. Tromborg, "Spectral linewidth of DFB lasers including the effect of spatial holeburning and nonuniform current injection," *IEEE Photon. Technol. Lett.*, vol. 2, pp. 312–315, 1990.
[32] ——, "Modulation characteristics of tunable DFB/DBR lasers with one or two passive tuning sections," *IEEE J. Quantum Electron.*, vol. 25, pp. 1254–1260, 1989.
[33] F. Libbrecht, G. Morthier, and R. Baets, and P. Lagasse, "Large-signal multi-mode DFB-laser model as part of an optical communication simulation tool," in *Proc. OFC'91*, San Diego, CA, Feb. 10, 1991, paper WM4, p. 120.
[34] P. J. Corvini and T. L. Koch, "Computer simulation of high-bit-rate optical fiber transmission using single-frequency lasers," *J. Lightwave Technol.*, vol. 5, pp. 1591–1595, 1987.
[35] J. C. Cartledge and J. S. Burley, "The effect of laser chirping on lightwave system performance," *J. Lightwave Technol.*, vol. 7, pp. 568–573, 1989.
[36] A. J. Lowery, "A new dynamic semiconductor laser model based on the transmission line modelling method," *IEE Proc. J. Optoelectron.*, vol. 134, pp. 281–289, 1987.
[37] R. S. Tucker, "High-speed modulation of semiconductor lasers," *J. Lightwave Technol.*, vol. LT-3, pp. 1180–1192, 1985.
[38] A. J. Lowery, "A new time-domain model for spontaneous emission in semiconductor lasers and its use in predicting their transient response," *Int. J. Numer. Model.*, vol. 1, pp. 153–164, 1988.
[39] ——, "A two-port bilateral model for semiconductor lasers," *IEEE J. Quantum Electron.*, vol. 28, pp. 82–92, Jan. 1992.
[40] K. Uomi, "Modulation-doped multi-quantum well (MD-MQW) lasers. I. Theory," *Japan. J. Appl. Phys.*, vol. 29, pp. 81–87, 1990.
[41] N. S. Bergano, "Wavelength discriminator method for measuring dynamic chirp in DFB lasers," *Electron. Lett.*, vol. 24, pp. 1296–1297, 1988.

Arthur J. Lowery, for a photograph and biography, see p. 92 of the January 1992 issue of this JOURNAL.

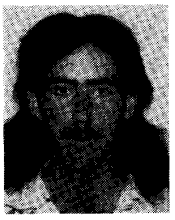

Adrian Keating was born in Melbourne, Australia, in 1967. He received the degree in electrical and electronic engineering from the University of Melbourne in 1989.

He has been involved with Telecom Australia since 1988, and has worked with Telecom Research Laboratories from 1990 to 1991 on cellular diversity schemes and laser modeling. He is currently pursuing the M.Sc. degree at the University of Melbourne and is conducting research into tunable laser sources.

Casper N. Murtonen was born in Melbourne, Australia, on July 15, 1968. He received the B.E. (Hons.) degree in electrical engineering from the University of Melbourne in April 1991.

He is currently working towards the Ph.D. degree at the University of Melbourne, where he is involved in numerical modeling of photonic devices and systems.

Mr. Murtonen is a member of Delta Nu Femto.